Active disturbance rejection control of an islanded PV/wind/battery microgrid with power quality enhancement by SAPF

Youssef Oubail[1], Imad Aboudrar[2], Mohamed El hafydy[1], Elmoutawakil Alaoui My Rachid[1], Elmahni Lahoussine[3]

[1]Laboratory of Engineering Sciences and Energy Management, ENSA AGADIR, Ibn Zohr University, Agadir, Morocco
[2]Engineering and Sustainable Development research team, EST of Dakhla, Ibn Zohr University, Dakhla, Morocco
[3]Renewable Materials and Energies Laboratory, Faculty of Sciences, Ibn Zohr University, Agadir, Morocco

Article Info

ABSTRACT

The focus in this study is on an islanded microgrid based on hybrid renewable energy sources and storage systems. This latter is considered as an essential element for all off-grid autonomous systems to offer a reliable and stable operation. The proposed system is composed of a photovoltaic system, a wind power system based on a synchronous generator and a storage system. The proposed control strategy is intended to control, through the load side converter (LSC), the AC bus voltage in terms of amplitude and frequency under different operating conditions, and to obtain, through the bi-directional battery side converter (BSC), a better regulation between the available production and the global load demand. The proposed strategy also contributes to the power quality improvement in the AC bus by controlling the PV inverter to work as a shunt active power filter to provide the required harmonic current component to non-linear loads. A new robust control strategy for internal current and voltage control loops is proposed in this research paper, it's the active disturbance rejection control (ADRC) and it is based on the extended state observer which allows to estimate all disturbances affecting the control, such as modeling errors and parameter variations.

Corresponding Author:

Youssef Oubail
Laboratory of Engineering Sciences and Energy Management, ENSA Agadir, Ibn Zohr University
Agadir, Morocco
Email: youssef.oubail@edu.uiz.ac.ma

1. INTRODUCTION

With the large-scale interconnection and expansion of the power network, the fragility of the traditional power system has become more prominent, and it cannot cope with the reliability and diversity needs of users. At the same time, the intensification of global environmental problems and the continuous reduction of fossil fuel reserves have promoted the rapid development of renewable energy power generation technology [1]. Distributed power generation units such as photovoltaic power generation systems, wind power generation systems, micro gas turbines, and fuel cell power generation systems are used in modern power systems [2] and the medium penetration rate continues to increase [3].

The concept of microgrid is proposed to effectively integrate and utilize renewable distributed generations (DGs), energy storage systems, electric vehicles, controllable loads and users at the medium and low voltage level [4]. One of the key characteristics of the microgrid is that it can be regarded as a

controllable entity from the perspective of the public grid. Relying on the point of common coupling (PCC) and switch, the microgrid system can run in grid-connected mode or island mode [5]. During grid-connected operation, it is necessary to achieve controllable tie-line power flow and maximize the use of renewable distributed power sources; In the island mode, the stable operation of the microgrid autonomous system needs to be ensured, it is called a weak microgrid due to the lack of inertia, and therefore it requires the introduction of a robust control system in order to form and maintain the constant voltage and frequency for any operating condition (grid forming) [6]. Therefore, in order to improve the reliability of the system, it is essential to integrate different sources of renewable energy working in a complementary way as wind and solar energy [7] and also to implement a robust control strategy to handle the different uncertainties and disturbances that can be faced in a complex microgrid [8].

In general, a range of traditional control methods, including PI/PID, sliding mode, and linear quadratic control with set parameters for a certain operating point, have been used in microgrid applications. With the control system parameters set to the recommended values in this situation, proper steady-state performance can be obtained. However, these techniques are only able to guarantee a satisfying dynamic performance compromise when the operating conditions are highly variable. As a result, it is necessary to update the control parameters [9]. Due to the low inertia, uncertainties, and intermittent nature of RES, one of the primary hurdles for autonomous microgrids is stability and control issues [10]. This calls for the creation of brand-new, cutting-edge control structures to maintain desired performance in face of unforeseen disturbances and model uncertainty. With only three parameters to optimize, PI/PID control may deliver good performance with a straightforward structure that is extensively applicable in industrial process systems. Nevertheless, due to complex systems and quick changes in operating points, the PI/PID controller with fixed gains is unable to handle the control difficulties [11]–[13]. In contrast to PI/PID control, which can have an ideal solution in terms of weighted matrices, the linear quadratic controller (LQR) is more stable and robust. However, it has some drawbacks, such as the requirement that all system states be measurably, the inability to manage system restrictions and disturbances, and the difficulty of obtaining an analytical answer to the Riccati equation [14]. Because it is robust to disturbances and model errors, sliding mode control (SMC) is preferable to the LQR approach. Although it occasionally exhibits poor performances in terms of uncertainties and mismatched load variations, its principal drawback is the chattering phenomena brought on by the discontinuous terms [15], [16]. Model predictive control (MPC) is a commonly used, quick computing system that can forecast how a system will behave dynamically over a finite time horizon and is immediately applicable to big and multivariate processes. Because it can manage state and control restrictions, variable interactions, and system complexity, it has an advantage over the LQR. The MPC's major drawback, meanwhile, is that it has to accurately identify the process model [17]. Additionally, because of its significant reliance on the model, it is unable to deal with unknown parameters, and performance analysis is therefore highly challenging. Particle swarm optimization (PSO), fuzzy logic, and neural networks are three examples of heuristic algorithms that have been extensively utilized for parameter tweaking and learning the behavior of dynamical systems. However, their fundamental flaw is that they only look for the almost ideal answer and are unable to keep the ideal solution [18]–[20]. In comparison to the aforementioned control strategies, the robust controllers as H_∞ control provide a number of advantages [21]. In fact, it is highly helpful when working with MIMO models, which can simultaneously satisfy a number of control objectives. However, it has certain downsides, including the requirement for adequate mathematical proficiency and the likelihood that it is unfeasible for large-scale systems [22], [23].

Based on the preceding research, we propose the ADRC control strategy in this paper as an optimal and robust solution to problems related to model uncertainties and external disturbances for Microgrid applications [24]. The ADRC system obtains the data about any disturbances directly from the input and output signals of the controlled system. It then promptly eliminates the disturbance by applying control adjustments. This proactive approach is superior to the traditional PID control method, which is considered passive in comparison. Imagine the disturbance as an illness, while PID control treats the symptoms, ADRC prevents it from occurring in the first place [25]. Currently, ADRC has been widely adopted in various fields, such as wind energy systems, robotics, and drone control [26]–[28].

The studied autonomous microgrid in this paper is illustrated in Figure 1. It is based on a 750 kW wind power conversion chain integrating storage batteries and on a 100 kW photovoltaic conversion chain. The suggested control system includes five distinct controllers, namely the machine converter (MSC) controller, load converter (LSC) controller, battery side converter (BSC) controller, PV chopper (PVC) controller, and the parallel active filter (SAPF) controller located on the photovoltaic system side. The MSC controller allows the wind turbine to operate in a way to extract the maximum power (MPPT) and to limit the power to its maximum value during gusts (pitch control). The LSC controller sustains the voltage amplitude and frequency in the AC bus, enabling stable performance under varying load conditions. The BSC controller manages the battery charging and discharging to keep the DC bus voltage consistent and balance the power generation and demand. The PVC controller allows the extraction of the maximum power and the SAPF controller provides the required

harmonic current components in the AC bus to reduce the THD and have a good power quality. The paper is summarized into four sections, with the first providing an overview of the article, the second introducing the modeling and design of the autonomous microgrid components, the third delving into the ADRC strategy and the design of the five controllers, and the fourth presenting simulation results and discussions.
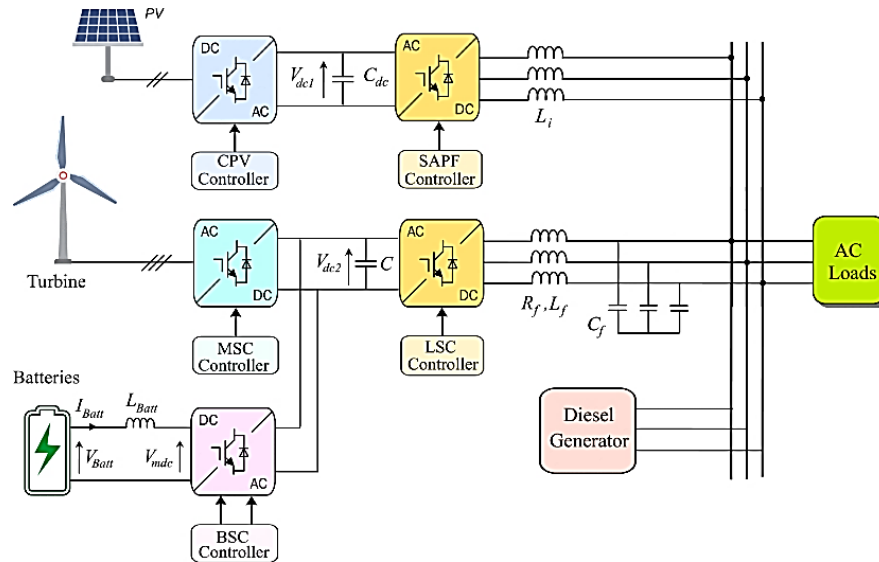

Figure 1. Topology of the proposed autonomous microgrid

2. DESING AND MODELING OF THE AUTONMOUS MICROGRID COMPONENTS

The studied system is based on two wind and photovoltaic conversion chains and on a battery storage system that allows to balance the generation and consumption of power, the photovoltaic conversion chain is controlled in a way to work as a parallel active filter in order to improve the power quality and to wind chain to supply the loads and charge the storage system in case of surplus. The modeling and design of the components utilized in this paper are presented in this section, the wind system and the PV system modeling are not given and they can be found in our previous paper [28].

2.1. Battery storage modeling

A general lead-acid battery model is utilized in this work since it is more feasible for renewable systems due to its low cost and wide availability. The lead-acid battery (LAB) is represented using the charge and discharge equations [29]:

$$V_{bat} = E - R_b i \tag{1}$$

$$E = E_0 - K \frac{Q}{Q-it} it - K \frac{Q}{Q-it} i^* + Exp(t) \tag{2}$$

$$E = E_0 - K \frac{Q}{Q-it} it - K \frac{Q}{it-0.1Q} i^* + Exp(t) \tag{3}$$

$$\frac{dExp(t)}{dt} = B|i(t)|(-Exp(t) + Au(t)) \tag{4}$$

The discharge model and the characteristic of the LAB storage system are given in Figure 2.

2.2. Battery side bidirectional converter design BSC

A buck-boost converter was chosen in this application to serve as a battery controller to connect the DC bus of the wind string to the storage battery. Its topology is simple with a reduced number of elements. The circuit consists of an inductor L_b, a capacitor C_b, and two IGBTs with antiparallel diodes that are controlled complementary to ensure current bidirectionality. It can operate as a step-down converter (switch S_1) in charge mode and as a step-up converter (switch S_2) in discharge mode. The circuit is shown in Figure 3. The parameters of L_b and C_b can be calculated as (5) and (6) [30].

$$L_b = \frac{V_{dc2} - V_b}{2\Delta i_L f_s} D_{buck} = \frac{V_b}{2\Delta i_L f_s} D_{boost} \tag{5}$$

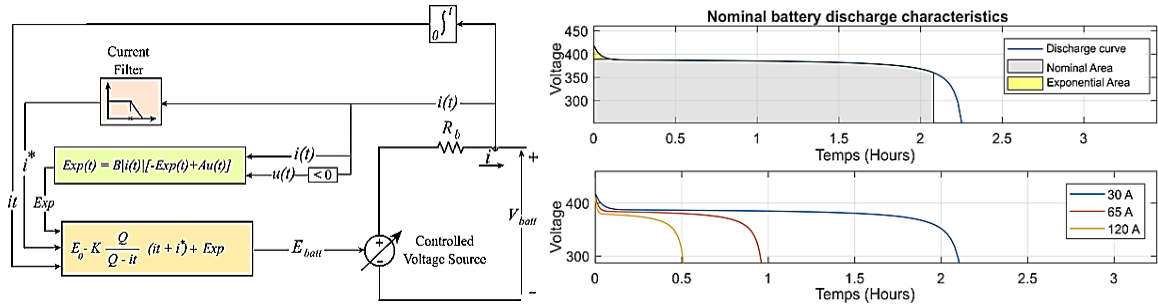$$C_b = \frac{\Delta i_L}{8\Delta v_c i_L f_s} \tag{6}$$

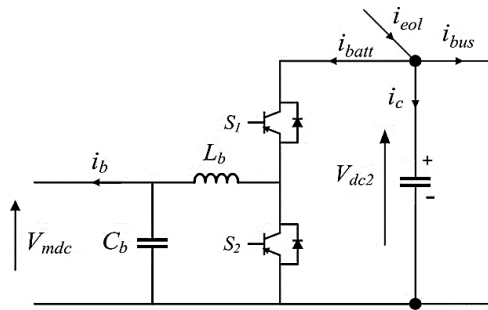Figure 2. The discharge model and the characteristic of the LAB storage system

Figure 3. Bidirectional converter circuit diagram

2.3. Load modeling

In this study, a dynamic load is used to illustrate the operation of balanced/linear type AC loads. It is formed by a resistor R_L and an inductance l_L, which are given by theses expressions as a function of the required active and reactive powers P_L and Q_L.

$$\begin{cases} R_L = \frac{V_c{}^2 P_L}{P_L{}^2 + Q_L{}^2} \\ X_L = L_L \omega_L = \frac{V_c{}^2 P_L}{P_L{}^2 + Q_L{}^2} \end{cases} \tag{7}$$

Also, a nonlinear load is considered in this study, in order to demonstrate the effectiveness of active filtering by SAPF, so a bridge rectifier with RL load is used.

2.4. Modeling the RLC filter

The conversion from the DC voltage supply of the wind turbine to AC power for the load is facilitated by a three-phase voltage source DC/AC converter, also known as an LSC. In order to produce a nearly sinusoidal voltage for the load, it is necessary to include an RLC filter between the LSC and the power receiver. The RLC filter, as depicted in Figure 1, can be represented through the following set of equations, disregarding mutual inductances.

$$\begin{cases} \frac{di_{df}}{dt} = -\frac{R_f}{L_f} i_{df} + \omega_L i_{qf} + \frac{1}{L_f} V_{di} - \frac{1}{L_f} V_{ds} \\ \frac{di_{qf}}{dt} = -\frac{R_f}{L_f} i_{qf} - \omega_L i_{df} + \frac{1}{L_f} V_{qi} - \frac{1}{L_f} V_{qs} \\ \frac{dV_{ds}}{dt} = \frac{1}{C_f} i_{df} + \omega_L V_{qs} - \frac{1}{C_f} i_{dL} \\ \frac{dV_{qs}}{dt} = \frac{1}{C_f} i_{qf} - \omega_L V_{ds} - \frac{1}{C_f} i_{qL} \end{cases} \tag{8}$$

3.   PROPOSED ADRC CONTROL STRATEGIES FOR THE FIVE CONVERTERS

The control strategy known as ADRC has been created by Han as a dependable solution to the problems associated with conventional PID control methods [24]. The ADRC approach is known for its robustness, despite the lack of clarity and predictability in the process model and controlling coefficients. The design of the ADRC regulator includes three key components: the tracking differentiator (TD), the extended state observer (ESO), and the non-linear state error feedback (NLSEF) control law. Depending on the design, the ADRC can be classified as linear or non-linear. For instance, if non-linear elements are included, it is referred to as non-linear ADRC, whereas if linear elements are used, it is referred to as linear ADRC. The structure of the ADRC regulator is depicted in Figure 4. The mathematical detail of the ADRC control can be found in our previous paper [28]. As mentioned earlier, the proposed control approach encompasses five key control circuits: the MSC controller, the CPV controller, the BSC controller, the LSC controller, and the SAPF controller. The functions and workings of each circuit will be explored in subsequent sections.
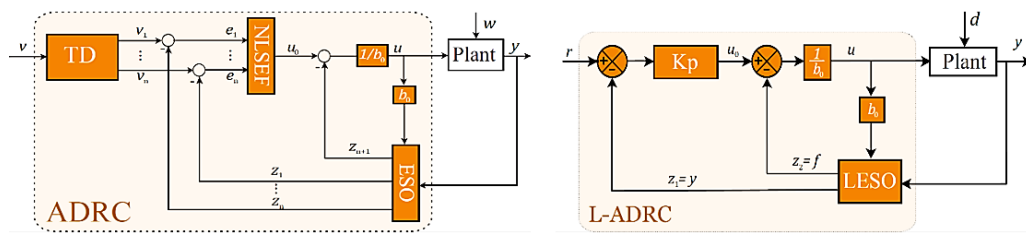

Figure 4. Bloc diagram of nonlinear and linear ADRC

3.1. MSC control circuit

The main objective of the machine-side converter control is to operate the synchronous wind turbine to extract the maximum power (MPPT) and limit the power to its maximum value during bursts (Pitch control), the detail of this control is already elaborated in our previous paper [28], where the linear ADRC is used to regulate the stator currents at their references, in such a way that the current i_{ds} is fixed at zero and the current i_{qs} follows its reference obtained by the OTC technique, moreover the value of the extracted power is controlled, through the pitch control actuator, in such a way as not to exceed the nominal power of the generator in case of strong wind speed. The equivalent control circuit is given in Figure 5.
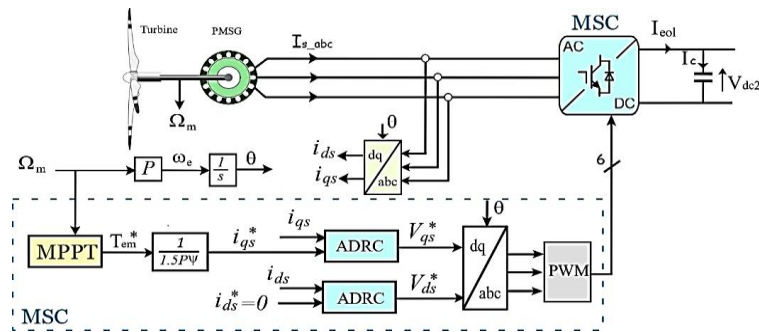

Figure 5. Proposed linear ADRC MSC control circuit

3.2. CPV control circuit

To achieve optimal operation of the photovoltaic string during climate change, the PV-side chopper is controlled to operate around the maximum power point, this is achieved by the two-stage control strategy [31]. An adaptive MPPT based algorithm is used to generate the reference voltage V_{MPP} which is then regulated by the linear ADRC controller. The control circuit is given in Figure 6. For more details about the design of this controller please refer to our previous paper [32].

3.3. BSC control circuit

The primary goal of this control is to manage the power flow of the batteries to maintain the wind source DC bus voltage and ensure power balance between production and demand. When a battery is drained,

the bi-directional converter on the battery side enters "boost" mode, allowing energy to flow from the battery to the DC bus. When the battery is charging, the bi-directional converter runs in "buck" mode, allowing power to flow from the DC bus to the battery. The BSC control circuit that was constructed for this work is depicted in Figure 7. The DC voltage is kept at a set level by an external control loop. The battery current reference is limited to a specific maximum or minimum current through the use of an ADRC controller (I_{batt}^{max} discharging and I_{batt}^{min} for charging). The charge current is limited based on the chemical properties of the battery, with a limit of $C/10$ for lead-acid batteries where C is the nominal capacity. The internal control loop, utilizing an ADRC controller, manages the battery current to reach its reference [33]. The direction of the current reference determines whether the system is in charge or discharge mode. If the reference is positive, the DC bus needs more power, causing the bi-directional converter to work in boost mode by draining the battery (Switch S_2). On the other hand, if the current reference is negative, an excess of power needs to be removed, and the bi-directional converter operates in step-down mode to charge the battery (Switch S_1) [34].
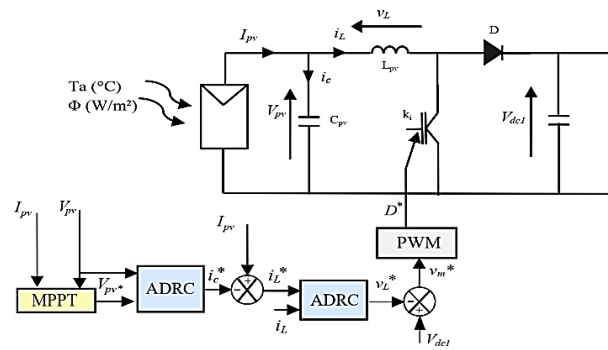

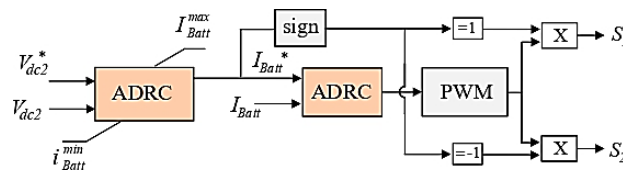Figure 6. DC-DC chopper linear ADRC based control

Figure 7. Proposed BSC ADRC based control circuit

In order to develop the ADRC controller of the external voltage loop, we establish the expression modeling the DC bus, and we have:

$$V_{dc2} = \frac{1}{C} \int i_c dt = \frac{1}{C} \int (i_{eol} - i_{bus} - i_{batt}) dt \tag{9}$$

neglecting the initial conditions, we have:

$$\frac{dV_{dc2}}{dt} = \frac{1}{C} (i_{eol} - i_{bus} - i_{batt}) \tag{10}$$

so, the ADRC controller is designed as follows:

$$\begin{cases} f_{V_{dc2}}(\cdot) = \frac{1}{C}(i_{eol} - i_{bus}) + \Delta(-\frac{1}{C}) \\ b_{0_{V_{dc2}}} = -\frac{1}{C} \\ u_{V_{dc2}} = i_{batt} \end{cases} \tag{11}$$

Similarly, for the internal current loop we express the equation connecting the storage batteries to the bidirectional converter through the inductive filter, hence the dynamic equation of the battery current is expressed as follows:

$$L_{batt} \frac{di_{batt}}{dt} = V_{batt} - V_{mdc} \tag{12}$$

and so, the ADRC controller corresponding to this equation is given by:

$$\begin{cases} f_{i_{batt}}(\cdot) = \frac{V_{batt}}{L_{batt}} + \Delta(-\frac{1}{L_{batt}}) \\ \quad b_{0_{i_{batt}}} = -\frac{1}{L_{batt}} \\ \quad u_{i_{batt}} = V_{mdc} \end{cases} \qquad (13)$$

3.4. LSC control circuit

A bi-directional DC-AC converter is used to connect the DC bus of the wind chain and the AC bus of the microgrid. The output terminals of this converter are connected to the AC bus by a coupling filter (L_f, C_f) whose voltage and current provided by the converter can be regulated. While the system studied here is a stand-alone microgrid that is not interconnected to the electrical grid, this converter is therefore controlled to behave as a voltage source with a determined voltage amplitude and frequency, this type of control is known as (grid forming) [35]. The control circuit implemented for this study is shown in Figure 8. The AC bus voltage is controlled during the variation of the power generated by the autonomous system or that required by the load. Therefore, we are interested in developing two control loops, an external voltage loop and an internal current loop.
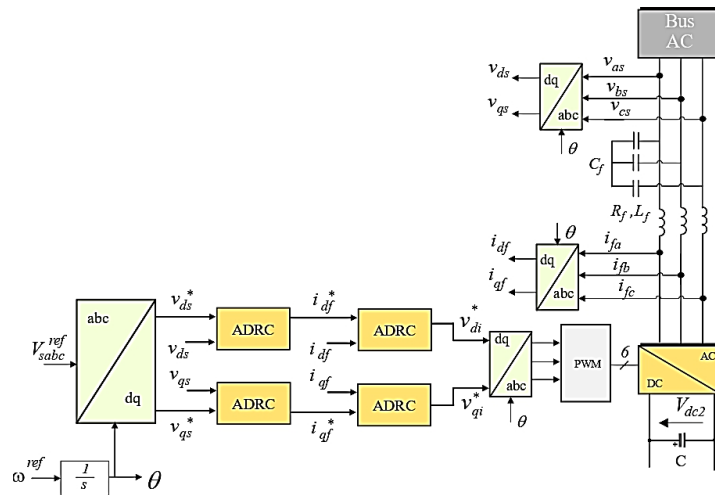

Figure 8. Proposed LSC based ADRC control

To design this control circuit, it is crucial to determine the references for the voltages and currents. The voltage references V_{dsr} and V_{qsr} are obtained by a park transformation of a 3-phase voltage with a frequency of 50Hz and an amplitude of 220V. The reference currents required by the load are given as (14).

$$\begin{cases} i_{dL}^{*} = \frac{P_L V_{dsr} + Q_L V_{qsr}}{V_{dsr}^2 + V_{qsr}^2} \\ i_{qL}^{*} = \frac{P_L V_{dsr} - Q_L V_{qsr}}{V_{dsr}^2 + V_{qsr}^2} \end{cases} \qquad (14)$$

According to the RLC filter model, the voltage equations in the d-q frame are given as follows:

$$\begin{cases} \frac{dV_{ds}}{dt} = \frac{1}{C_f} i_{df} + \omega_L V_{qs} - \frac{1}{C_f} i_{dL} \\ \frac{dV_{qs}}{dt} = \frac{1}{C_f} i_{qf} - \omega_L V_{ds} - \frac{1}{C_f} i_{qL} \end{cases} \qquad (15)$$

These expressions correspond to the canonical form of the ADRC and thus, the controllers can be designed as follows:
− For the d-axis:

$$\begin{cases} f_{V_{ds}}(\cdot) = \omega_L V_{qs} - \frac{1}{C_f} i_{dL} + \Delta(\frac{1}{C_f}) \\ \quad\quad b_{0_{V_{ds}}} = \frac{1}{C_f} \\ \quad\quad u_{V_{ds}} = i_{df} \end{cases} \tag{16}$$

− For the q-axis:

$$\begin{cases} f_{V_{qs}}(\cdot) = -\omega_L V_{ds} - \frac{1}{C_f} i_{qL} + \Delta(\frac{1}{C_f}) \\ \quad\quad b_{0_{V_{qs}}} = \frac{1}{C_f} \\ \quad\quad u_{V_{qs}} = i_{qf} \end{cases} \tag{17}$$

Thus, the expressions of the circulating currents in the RLC filter are expressed as (18).

$$\begin{cases} \frac{di_{df}}{dt} = -\frac{R_f}{L_f} i_{df} + \omega_L i_{qf} + \frac{1}{L_f} V_{di} - \frac{1}{L_f} V_{ds} \\ \frac{di_{qf}}{dt} = -\frac{R_f}{L_f} i_{qf} - \omega_L i_{df} + \frac{1}{L_f} V_{qi} - \frac{1}{L_f} V_{qs} \end{cases} \tag{18}$$

So, the corresponding ADRC regulators are given by:
− For the d-axis:

$$\begin{cases} f_{i_{df}}(\cdot) = -\frac{R_f}{L_f} i_{df} + \omega_L i_{qf} - \frac{1}{L_f} V_{ds} + \Delta(\frac{1}{L_f}) \\ \quad\quad b_{0_{i_{df}}} = \frac{1}{L_f} \\ \quad\quad u_{i_{df}} = V_{di} \end{cases} \tag{19}$$

− For the q-axis:

$$\begin{cases} f_{i_{qf}}(\cdot) = -\frac{R_f}{L_f} i_{qf} - \omega_L i_{df} - \frac{1}{L_f} V_{qs} + \Delta(\frac{1}{L_f}) \\ \quad\quad b_{0_{i_{qf}}} = \frac{1}{L_f} \\ \quad\quad u_{i_{qf}} = V_{qi} \end{cases} \tag{20}$$

3.5. SAPF control circuit

The main objective of this controller is to provide the required current harmonic components in the AC bus in order to reduce the THD and have a good power quality. To do this, the DC/AC converter of the photovoltaic chain is controlled to work as a parallel active filter (SAPF), its operating principle is to generate harmonic currents in phase opposition to those existing in the AC bus of the autonomous microgrid. To do this, several control techniques have been proposed in the literature, in this thesis, we are interested in the control technique known as P-Q Theory proposed by Akagi and Nabae [36]. The working principle of this control algorithm is detailed below and the different steps to obtain the harmonic components of the current are illustrated in Figure 9. This technique relies on the measurement of the three-phase momentary variables in the AC bus of the microgrid, the voltage and the load currents are detected and transformed into a fixed two-phase coordinate system ($\alpha - \beta$) (Clarke's transformation) [37].

The governing equations of this transformation are given by the following expressions [36]:

$$\begin{bmatrix} v_{\alpha s} \\ v_{\beta s} \end{bmatrix} = \sqrt{\frac{2}{3}} \begin{bmatrix} 1 & -\frac{1}{2} & -\frac{1}{2} \\ 0 & \frac{\sqrt{3}}{2} & -\frac{\sqrt{3}}{2} \end{bmatrix} \begin{bmatrix} v_{as} \\ v_{bs} \\ v_{cs} \end{bmatrix} \tag{21}$$

$$\begin{bmatrix} i_{\alpha L} \\ i_{\beta L} \end{bmatrix} = \sqrt{\frac{2}{3}} \begin{bmatrix} 1 & -\frac{1}{2} & -\frac{1}{2} \\ 0 & \frac{\sqrt{3}}{2} & -\frac{\sqrt{3}}{2} \end{bmatrix} \begin{bmatrix} i_{aL} \\ i_{bL} \\ i_{cL} \end{bmatrix} \tag{22}$$

The vectors of voltage and current are:

$$\vec{v} = v_{\alpha s} + jv_{\beta s} \tag{23}$$

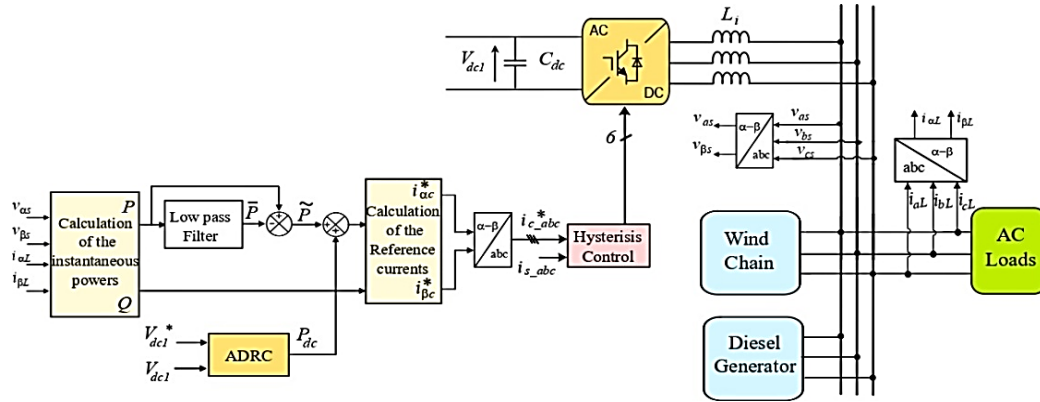$$\vec{i} = i_{\alpha L} + ji_{\beta L} \tag{24}$$

Figure 9. SAPF ADRC control based on the P-Q theory algorithm

Therefore, by taking into account the complex power $S = \vec{v}\vec{i}$, and considering the previous transformations, the active power P the and the reactive power Q can be determined by [37]:

$$\begin{bmatrix} P \\ Q \end{bmatrix} = \begin{bmatrix} v_{\alpha s} & v_{\beta s} \\ -v_{\beta s} & v_{\alpha s} \end{bmatrix} \begin{bmatrix} i_{\alpha L} \\ i_{\beta L} \end{bmatrix} \tag{25}$$

Replacing the α-β voltages and currents by their equivalent values, we have:

$$P = v_{\alpha s} i_{\alpha L} + v_{\beta s} i_{\beta L} = v_{as} i_{aL} + v_{bs} i_{bL} + v_{cs} i_{cL} \tag{26}$$

$$Q = v_{\alpha s} i_{\beta L} - v_{\beta s} i_{\alpha L} = -\frac{1}{\sqrt{3}} [(v_{as} - v_{bs})i_{cL} + (v_{bs} - v_{cs})i_{aL} + (v_{cs} - v_{as})i_{bL}] \tag{27}$$

from the (25), we put:

$$\Delta = v_{\alpha s}{}^2 + v_{\beta s}{}^2 \tag{28}$$

and we obtain:

$$\begin{bmatrix} i_{\alpha L} \\ i_{\beta L} \end{bmatrix} = \frac{1}{\Delta} \begin{bmatrix} v_{\alpha s} & -v_{\beta s} \\ v_{\beta s} & v_{\alpha s} \end{bmatrix} \begin{bmatrix} P \\ Q \end{bmatrix} \tag{29}$$

where:

$$\begin{bmatrix} i_{\alpha L} \\ i_{\beta L} \end{bmatrix} = \frac{1}{\Delta} \left\{ \begin{bmatrix} v_{\alpha s} & -v_{\beta s} \\ v_{\beta s} & v_{\alpha s} \end{bmatrix} \begin{bmatrix} P \\ 0 \end{bmatrix} + \begin{bmatrix} v_{\alpha s} & -v_{\beta s} \\ v_{\beta s} & v_{\alpha s} \end{bmatrix} \begin{bmatrix} 0 \\ Q \end{bmatrix} \right\} = \begin{bmatrix} i_{\alpha PL} \\ i_{\beta PL} \end{bmatrix} + \begin{bmatrix} i_{\alpha QL} \\ i_{\beta QL} \end{bmatrix} \tag{30}$$

with:

$$i_{\alpha PL} = \frac{v_{\alpha s}}{\Delta} P; \ i_{\alpha QL} = -\frac{v_{\beta s}}{\Delta} Q; \ i_{\beta PL} = \frac{v_{\beta s}}{\Delta} P; \ i_{\beta QL} = \frac{v_{\alpha s}}{\Delta} Q$$

when the voltages are sinusoidal and supply a non-linear load, as is the case in our system, the powers P and Q can be given as follows:

$$\begin{cases} P = \bar{P} + \tilde{P} \\ Q = \bar{Q} + \tilde{Q} \end{cases} \tag{31}$$

with, $\bar{P}$, $\bar{Q}$ are the average active and reactive powers related to the fundamental component of the current, $\tilde{P}$, $\tilde{Q}$ are the oscillating powers related to the harmonic component of the current. Considering equations (29) and (30), we can separate the current in the $(\alpha - \beta)$ frame to the sum of three current components. The active and reactive elements related to the fundamental frequency and the component related to harmonics. This results [37]:

$$\begin{bmatrix} i_{\alpha L} \\ i_{\beta L} \end{bmatrix} = \underbrace{\frac{1}{\Delta}\begin{bmatrix} v_{\alpha s} & -v_{\beta s} \\ v_{\beta s} & v_{\alpha s} \end{bmatrix}\begin{bmatrix} \bar{P} \\ 0 \end{bmatrix}}_{Active\_Current} + \underbrace{\frac{1}{\Delta}\begin{bmatrix} v_{\alpha s} & -v_{\beta s} \\ v_{\beta s} & v_{\alpha s} \end{bmatrix}\begin{bmatrix} \bar{Q} \\ 0 \end{bmatrix}}_{Reactive\_Current} + \underbrace{\frac{1}{\Delta}\begin{bmatrix} v_{\alpha s} & -v_{\beta s} \\ v_{\beta s} & v_{\alpha s} \end{bmatrix}\begin{bmatrix} \tilde{P} \\ \tilde{Q} \end{bmatrix}}_{Harmonic\_Current} \tag{32}$$

To counteract the reactive power and harmonic currents generated by the nonlinear loads, the reference signal for the parallel active filter must encompass the reactive current and the harmonic current. Also, to compensate for the switching losses in the converter and to keep its DC bus voltage constant, the SAPF consumes a small amount of active power (P_{dc}) that must be taken into account when generating the reference currents. This value is obtained through the regulation of the DC bus voltage by the ADRC regulator [38]. As a result, the reference currents are:

$$\begin{bmatrix} i_{\alpha c}{}^* \\ i_{\beta c}{}^* \end{bmatrix} = \frac{1}{\Delta}\begin{bmatrix} v_{\alpha s} & -v_{\beta s} \\ v_{\beta s} & v_{\alpha s} \end{bmatrix}\begin{bmatrix} \tilde{P} + P_{dc} \\ \bar{Q} + \tilde{Q} \end{bmatrix} \tag{33}$$

Applying the inverse Clark transformation, the reference compensation currents are:

$$\begin{bmatrix} i_{ac}{}^* \\ i_{bc}{}^* \\ i_{cc}{}^* \end{bmatrix} = \sqrt{\frac{2}{3}}\begin{bmatrix} 1 & 0 \\ -\frac{1}{2} & \frac{\sqrt{3}}{2} \\ -\frac{1}{2} & -\frac{\sqrt{3}}{2} \end{bmatrix}\begin{bmatrix} i_{\alpha c}{}^* \\ i_{\beta c}{}^* \end{bmatrix} \tag{34}$$

To isolate one of the three components, such as harmonic currents, it is necessary to differentiate the oscillating parts of the active and reactive powers from their steady parts [39]. This differentiation can be achieved by utilizing one of the two filtering devices depicted in Figure 10.

The relationship between the active power absorbed by the capacitor and the voltage at its terminals, which is necessary for the design of the ADRC controller for the DC bus voltage, is given by (35).

$$P_{dc} = \frac{dW_{dc}}{dt} = \frac{d}{dt}\left(\frac{1}{2}C_{dc}V_{dc1}{}^2\right) \tag{35}$$

This equation is adapted to the canonical form of the ADRC:

$$\frac{dV_{dc1}{}^2}{dt} = \frac{2}{C_{dc}}P_{dc} \tag{36}$$

and we get:

$$\begin{cases} f_{V_{dc1}}(\cdot) = \Delta\left(\frac{2}{C_{dc}}\right) \\ b_{V_{dc1}} = \frac{2}{C_{dc}} \\ u_{V_{dc1}} = P_{dc} \end{cases} \tag{37}$$
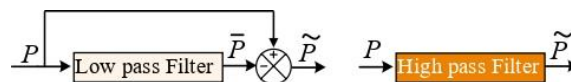

Figure 10. Filters used to extract Oscillating components

4. RESULTS AND DISCUSSION

In order to verify the efficiency of the proposed configuration, an extensive simulation was performed in MATLAB/Simulink software for different operating conditions. The solar radiation profile was modified in time to emulate the comportment of the sunlight and also the wind speed profile. Similarly, the AC linear load was also modified while taking into account the case of a non-linear load modeled by a three-phase bridge

rectifier, to analyze the response of the system to these variations as it would occur in a real microgrid. The wind and irradiation profiles applied in this simulation are shown in Figure 11. The linear load is applied as a dynamic load $R - L$. The starting value of the active and reactive power of this load is 200 kW and 50 kVAR respectively. At $t = 0.75 s$, the nonlinear load has been applied and it consumes an active power of 113 kW and reactive power of 50 kVAR. At $t = 1.3 s$, the nonlinear load was eliminated and the linear load was increased to 600 kW and 150 kVAR, at $t = 2 s$ the load is decreased to 500 kW and 150 kVAR.

Figure 12 shows the different powers exchanged in the autonomous microgrid. Figures 12(a) and 12(b) illustrates the powers extracted by the PV string and by the wind turbine for the applied wind and irradiation profiles. As can be seen in Figure 12(c) all the power extracted by the PV system is transferred by the parallel active filter to the AC bus in order to overdrive the demand while the AC-DC converter on the wind turbine side injects the additional power requested by the load as can be seen by Figures 12(d) and 12(e). When the wind system produces enough energy to supply the loads, the excess energy is stored by charging the battery. This can be observed in the battery power depicted in Figure 12(g), where a negative value indicates that energy is flowing from the DC bus to the battery. Conversely, when the wind turbine is unable to produce enough power to meet the demands of the loads, the battery must provide the supplementary power needed to satisfy these demands.
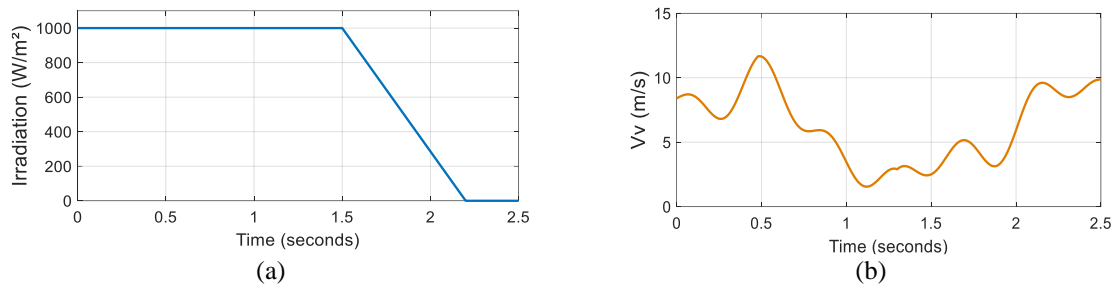

Figure 11. The wind and irradiation profiles applied: (a) irradiance profile and (b) wind profile
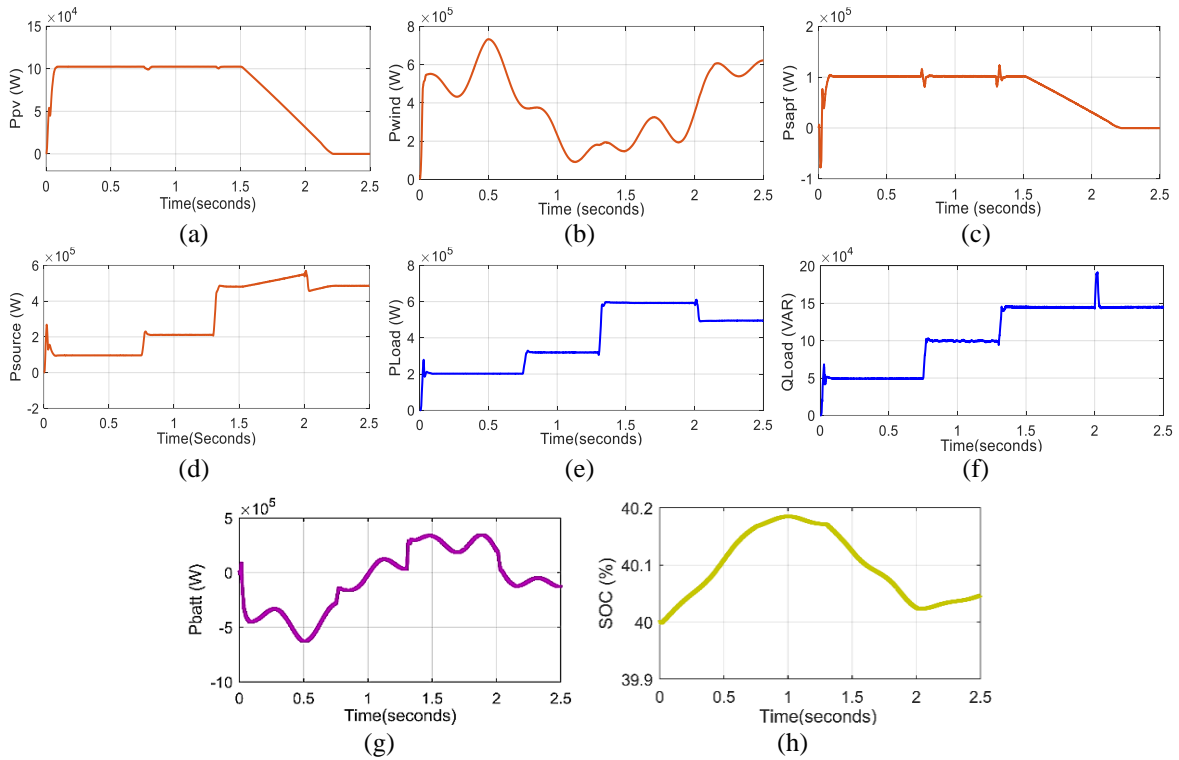

Figure 12. Active and reactive power exchanged in the microgrid, (a) PV power, (b) wind power, (c) SAPF power, (d) hybrid system power, (e) load active power, (f) load reactive power, (g) battery power, and (h) SOC

The Figure 13 shows the AC bus voltage and currents flowing in the autonomous microgrid. As can be seen in Figures 13(a) and 13(b), the AC bus voltage is kept constant for the different operating cases, hence it presents the characteristic of a three-phase voltage source having an amplitude of 311 V and frequency of 50 Hz and a phase shift of $2\pi/3$. The Figures 13(c) and 13(d) present the current required by the loads, we see that as soon as the nonlinear load is applied at the time t = 0.75 s, this current is distorted which will normally affect the source current I_{sabc}, but as can be seen from Figure 13(f), the parallel active filter injects a harmonic current in phase opposition to the one consumed in order to compensate for the harmonics in the AC bus.
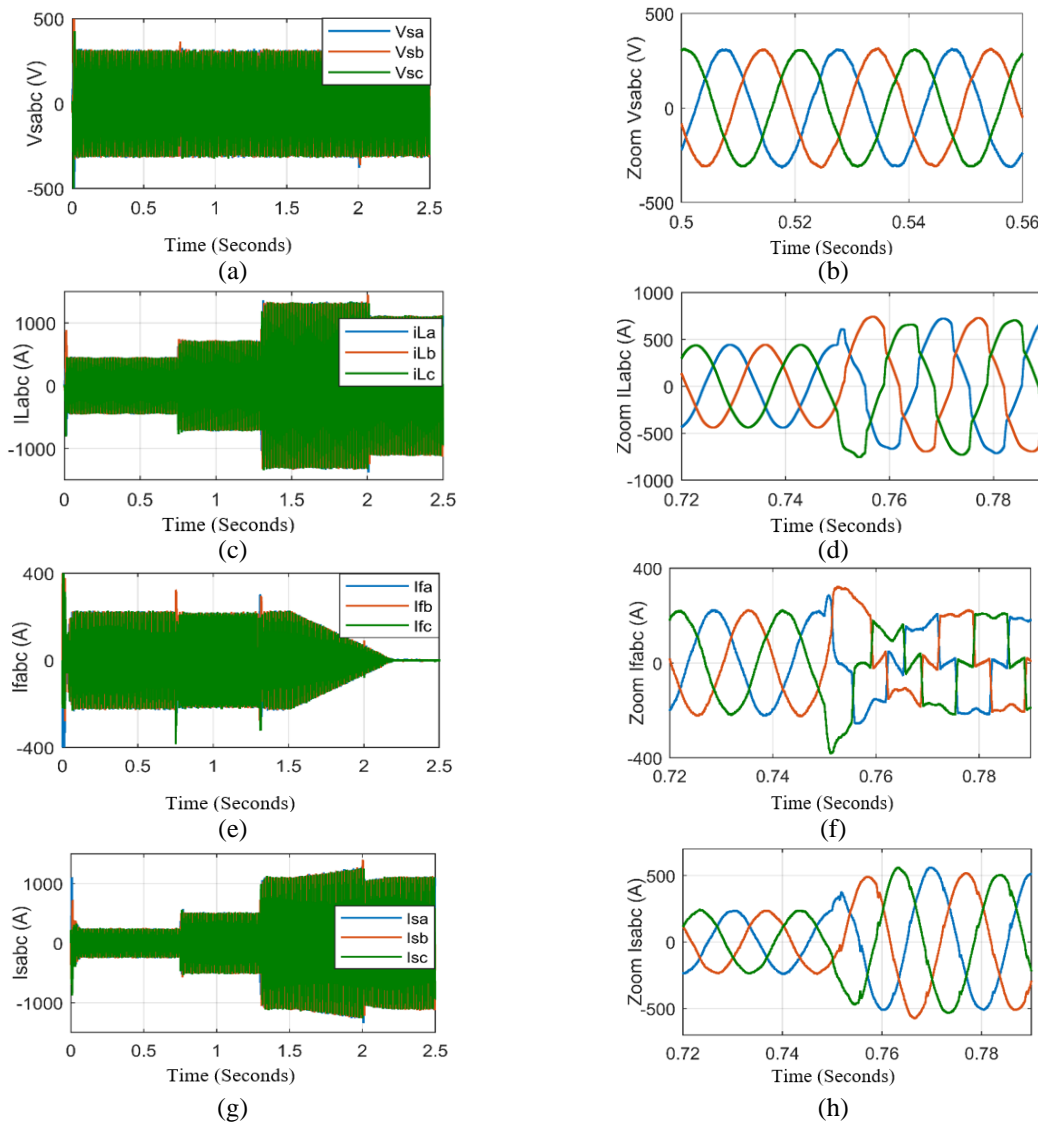
Figure 13. Voltage and current flowing in AC bus, (a) AC bus output voltage, (b) Vsabc zoom, (c) AC load currents, (d) ILabc zoom, (e) filter injected currents, (f) Ifabc zoom, (g) AC bus currents, and (h) Isabc zoom

The Figure 14 presents the results of the different regulation loops for the five controllers presented previously, as we can see the voltage of the DC bus of the two wind and photovoltaic conversion chains has been maintained observed during the different cases of operation, moreover we can see that the voltages V_{ds}, V_{qs} and the currents i_{df}, i_{qf} and i_{batt} have been regulated to their reference values by the different ADRC controllers. It can also be seen that the frequency of the AC bus voltages is maintained at 50 Hz for the different cases of power generation and consumption.
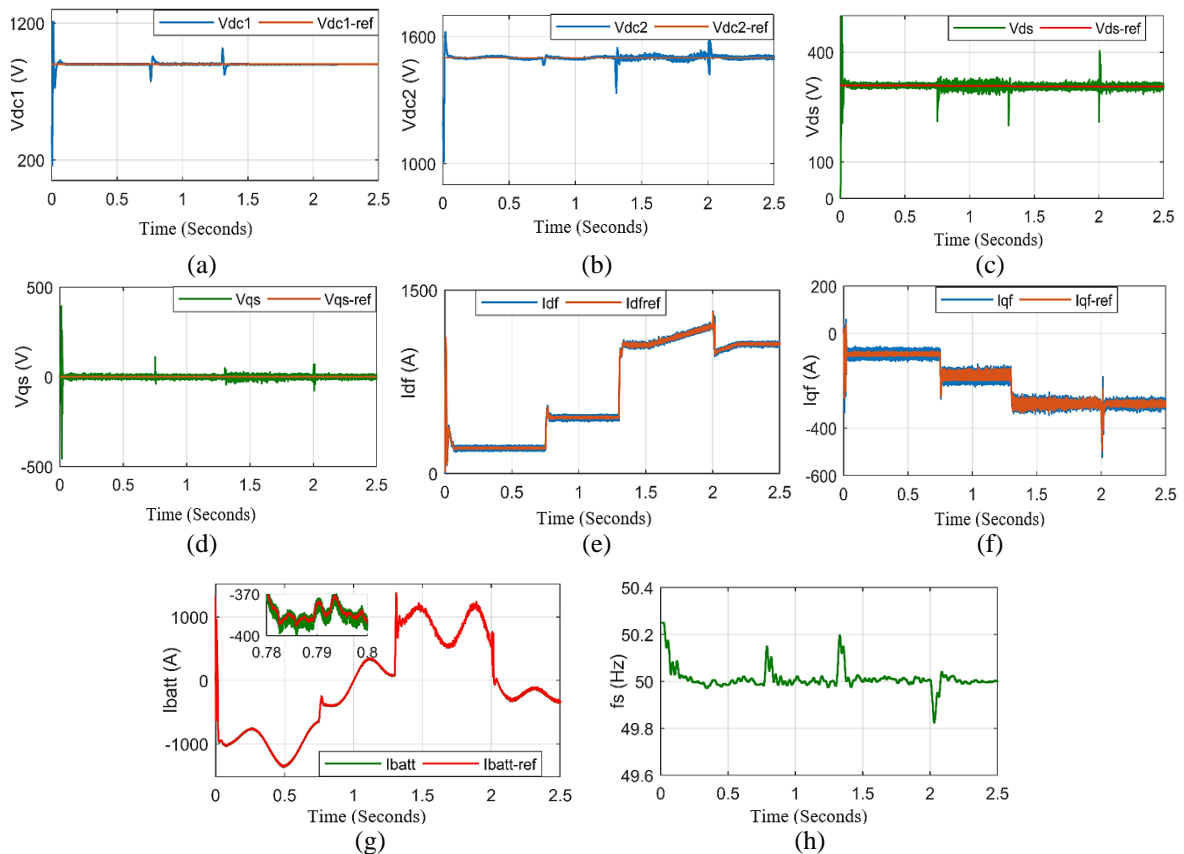
Figure 14. Results of the different control loops by ADRC, (a) SAPF DC bus voltage regulation,
(b) hybrid system DC bus voltage regulation, (c) d-axis voltage regulation, (d) q-axis voltage regulation,
(e) d-axis current regulation, (f) q-axis current regulation, (g) battery current regulation,
and (h) regulated AC bus frequency

5. CONCLUSION

In this paper, a new control strategy based on the ADRC controller for an isolated microgrid is presented. The objective of this control strategy is to form and maintain the constant voltage and frequency for any operating condition. The studied system is based on two renewable energy sources, wind and photovoltaic, and on a storage, system based on batteries in order to maintain the balance between production and consumption and thus improve the system performance, especially during transient periods. Additionally, the proposed control strategy enhances the power quality of the system by regulating the photovoltaic system to function as an active filter and supply the harmonic current component demanded by the nonlinear load. The effectiveness of this control strategy has been evaluated under a variety of operating conditions and has demonstrated its robustness in real autonomous microgrid environment conditions.

REFERENCES

[1] H. Schandl *et al.,* "Decoupling global environmental pressure and economic growth: scenarios for energy use, materials use and carbon emissions," *Journal of Cleaner Production*, vol. 132, pp. 45–56, Sep. 2016, doi: 10.1016/j.jclepro.2015.06.100.
[2] V. Khare, S. Nema, and P. Baredar, "Solar–wind hybrid renewable energy system: A review," *Renewable and Sustainable Energy Reviews*, vol. 58, pp. 23–33, May 2016, doi: 10.1016/j.rser.2015.12.223.
[3] E. Kabalci, "Design and analysis of a hybrid renewable energy plant with solar and wind power," *Energy Conversion and Management*, vol. 72, pp. 51–59, Aug. 2013, doi: 10.1016/j.enconman.2012.08.027.
[4] F. R. Badal, P. Das, S. K. Sarker, and S. K. Das, "A survey on control issues in renewable energy integration and microgrid," *Protection and Control of Modern Power Systems*, vol. 4, no. 1, Apr. 2019, doi: 10.1186/s41601-019-0122-8.
[5] R. Majumder, "Some aspects of stability in microgrids," *IEEE Transactions on Power Systems*, vol. 28, no. 3, pp. 3243–3252, Aug. 2013, doi: 10.1109/TPWRS.2012.2234146.
[6] P. Borazjani, N. I. A. Wahab, H. B. Hizam, and A. B. C. Soh, "A review on microgrid control techniques," *2014 IEEE Innovative Smart Grid Technologies - Asia (ISGT ASIA)*, May 01, 2014, doi: 10.1109/ISGT-Asia.2014.6873886.
[7] S. A. Mohamed, "Multi-input rectifier stage for a system of hybrid PV/wind driven PMSG," *SN Applied Sciences*, vol. 1, no. 12, Nov. 2019, doi: 10.1007/s42452-019-1629-3.
[8] V. Kumar, A. S. Pandey, and S. K. Sinha, "Grid integration and power quality issues of wind and solar energy system: A review,"

2016 International Conference on Emerging Trends in Electrical Electronics & Sustainable Energy Systems (ICETEESES), Mar. 01, 2016, doi: 10.1109/ICETEESES.2016.7581355.

[9] T. L. Vandoorn, J. D. M. De Kooning, B. Meersman, and L. Vandevelde, "Review of primary control strategies for islanded microgrids with power-electronic interfaces," *Renewable and Sustainable Energy Reviews*, vol. 19, pp. 613–628, Mar. 2013, doi: 10.1016/j.rser.2012.11.062.

[10] M. S. Mahmoud, N. M. Alyazidi, and M. I. Abouheaf, "Adaptive intelligent techniques for microgrid control systems: A survey," *International Journal of Electrical Power & Energy Systems*, vol. 90, pp. 292–305, Sep. 2017, doi: 10.1016/j.ijepes.2017.02.008.

[11] A. Ghosh, A. K. Ray, Md. Nurujjaman, and M. Jamshidi, "Voltage and frequency control in conventional and PV integrated power systems by a particle swarm optimized Ziegler–Nichols based PID controller," *SN Applied Sciences*, vol. 3, no. 3, Feb. 2021, doi: 10.1007/s42452-021-04327-8.

[12] M. H. Khooban, and T. Niknam, "A new intelligent online fuzzy tuning approach for multi-area load frequency control: Self Adaptive Modified Bat Algorithm," *International Journal of Electrical Power & Energy Systems*, vol. 71, pp. 254–261, Oct. 2015, doi: 10.1016/j.ijepes.2015.03.017.

[13] D. E. Olivares *et al.*, "Trends in microgrid control," *IEEE Transactions on Smart Grid*, vol. 5, no. 4, pp. 1905–1919, Jul. 2014, doi: 10.1109/tsg.2013.2295514.

[14] H. Keshtkar, F. D. Mohammadi, J. Ghorbani, J. Solanki, and A. Feliachi, "Proposing an improved optimal LQR controller for frequency regulation of a smart microgrid in case of cyber intrusions," *2014 IEEE 27th Canadian Conference on Electrical and Computer Engineering (CCECE)*, May 01, 2014, doi: 10.1109/CCECE.2014.6901017.

[15] S. Mishra, D. Ramasubramanian, and P. C. Sekhar, "A seamless control methodology for a grid connected and isolated PV-diesel microgrid," *IEEE Transactions on Power Systems*, vol. 28, no. 4, pp. 4393–4404, Nov. 2013, doi: 10.1109/tpwrs.2013.2261098.

[16] Y. Krim, D. Abbes, S. Krim, and M. Faouzi Mimouni, "Power management and second-order sliding mode control for standalone hybrid wind energy with battery energy storage system," *Proceedings of the Institution of Mechanical Engineers, Part I: Journal of Systems and Control Engineering*, vol. 232, no. 10, pp. 1389–1411, Jul. 2018, doi: 10.1177/0959651818784320.

[17] Y. Wang, Z. Chen, X. Wang, Y. Tian, Y. Tan, and C. Yang, "An estimator-based distributed voltage-predictive control strategy for AC islanded microgrids," *IEEE Transactions on Power Electronics*, vol. 30, no. 7, pp. 3934–3951, Jul. 2015, doi: 10.1109/TPEL.2014.2345696.

[18] H. Bevrani, F. Habibi, P. Babahajyani, M. Watanabe, and Y. Mitani, "Intelligent frequency control in an AC microgrid: online PSO-based fuzzy tuning approach," *IEEE Transactions on Smart Grid*, vol. 3, no. 4, pp. 1935–1944, Dec. 2012, doi: 10.1109/TSG.2012.2196806.

[19] R. M. Kamel, A. Chaouachi, and K. Nagasaka, "Three control strategies to improve the microgrid transient dynamic response during isolated mode: a comparative study," *IEEE Transactions on Industrial Electronics*, vol. 60, no. 4, pp. 1314–1322, Apr. 2013, doi: 10.1109/TIE.2012.2209609.

[20] Y. A.-R. I. Mohamed and E. F. El-Saadany, "Adaptive discrete-time grid-voltage sensorless interfacing scheme for grid-connected DG-inverters based on neural-network identification and deadbeat current regulation," *IEEE Transactions on Power Electronics*, vol. 23, no. 1, pp. 308–321, Jan. 2008, doi: 10.1109/tpel.2007.911879.

[21] A. Goodarzi, A. M. Ranjbar, M. Dehghani, M. GhasemiGarpachi, and M. Ghiasi, "Doubly fed induction generators to enhance inter-area damping based on a Robust controller: $ H_2/H_{\infty} $ Control," *SN Applied Sciences*, vol. 3, no. 1, Jan. 2021, doi: 10.1007/s42452-021-04150-1.

[22] M. Zadehbagheri, M. Pishavaie, R. Ildarabadi, and T. Sutikno, "The coordinated control of FACTS and HVDC using h-infinity robust method to stabilize the inter-regional oscillations in power systems," *International Journal of Power Electronics and Drive Systems (IJPEDS)*, vol. 8, no. 3, pp. 1274–1284, Sep. 2017, doi: 10.11591/ijpeds.v8.i3.pp1274-1284.

[23] S. R. Mohanty, N. Kishor, and P. K. Ray, "Robust H-infinite loop shaping controller based on hybrid PSO and harmonic search for frequency regulation in hybrid distributed generation system," *International Journal of Electrical Power & Energy Systems*, vol. 60, pp. 302–316, Sep. 2014, doi: 10.1016/j.ijepes.2014.03.012.

[24] J. Han, "From PID to active disturbance rejection control," *IEEE Transactions on Industrial Electronics*, vol. 56, no. 3, pp. 900–906, Mar. 2009, doi: 10.1109/tie.2008.2011621.

[25] Z.-L. Zhao and B.-Z. Guo, "On convergence of nonlinear active disturbance rejection control for SISO nonlinear systems," *Journal of Dynamical and Control Systems*, vol. 22, no. 2, pp. 385–412, Nov. 2015, doi: 10.1007/s10883-015-9304-5.

[26] Y. Meng, B. Liu, and L. Wang, "Speed control of PMSM based on an optimized ADRC controller," *Mathematical Problems in Engineering*, vol. 2019, pp. 1–18, May 2019, doi: 10.1155/2019/1074702.

[27] Z. Gao, "Scaling and bandwidth-parameterization based controller tuning," *Proceedings of the 2003 American Control Conference*, 2003., 2022, doi: 10.1109/acc.2003.1242516.

[28] I. Aboudrar, S. El Hani, M. S. Heyine, and N. Naseri, "Dynamic modeling and robust control by ADRC of Grid-Connected Hybrid PV-Wind Energy Conversion System," *Mathematical Problems in Engineering*, vol. 2019, p. e8362921, Oct. 2019, doi: 10.1155/2019/8362921.

[29] J. F. Manwell and J. G. McGowan, "Lead acid battery storage model for hybrid energy systems," *Solar Energy*, vol. 50, no. 5, pp. 399–405, May 1993, doi: 10.1016/0038-092x(93)90060-2.

[30] O. Tremblay and Louis-A. Dessaint, "Experimental validation of a battery dynamic model for EV applications," *World Electric Vehicle Journal*, vol. 3, no. 2, pp. 289–298, Jun. 2009, doi: 10.3390/wevj3020289.

[31] A. Chalh, S. Motahhir, A. E. Ghzizal, A. E. Hammoumi, and A. Derouich, "Global MPPT of photovoltaic system based on scanning method under partial shading condition," *SN Applied Sciences*, vol. 2, no. 4, Mar. 2020, doi: 10.1007/s42452-020-2580-z.

[32] I. Aboudrar, S. El Hani, H. Mediouni, N. Naseri, and A. Daghouri, "LVRT capability enhancement of a grid connected three phase PV system by ADRC and DSOGI FLL," *International Transactions on Electrical Energy Systems*, vol. 31, no. 11, Aug. 2021, doi: 10.1002/2050-7038.13059.

[33] I. Aboudrar, S. E. Hani, K. El Harouri, J. Martins, and R. J. Goncalves, "Reactive power compensation by ADRC in vehicle to grid application during grid fault conditions," *2020 International Conference on Electrical and Information Technologies (ICEIT)*, Mar. 01, 2020, doi: 10.1109/ICEIT48248.2020.9113222.

[34] S. Ferahtia, A. Djerioui, S. Zeghlache, and A. Houari, "A hybrid power system based on fuel cell, photovoltaic source and supercapacitor," *SN Applied Sciences*, vol. 2, no. 5, Apr. 2020, doi: 10.1007/s42452-020-2709-0.

[35] A. Vinayagam, K. S. V. Swarna, S. Y. Khoo, A. T. Oo, and A. Stojcevski, "PV based microgrid with grid-support grid-forming inverter control-(simulation and analysis)," *Smart Grid and Renewable Energy*, vol. 08, no. 01, pp. 1–30, 2017, doi: 10.4236/sgre.2017.81001.

[36] H. Akagi and A. Nabae, "The p-q theory in three-phase systems under non-sinusoidal conditions," *European Transactions on Electrical Power*, vol. 3, no. 1, pp. 27–31, Sep. 2007, doi: 10.1002/etep.4450030106.

[37] I. Aboudrar, S. E. Hani, H. Mediouni, and A. Aghmadi, "Active disturbance rejection control of shunt active power filter based on p-q theory," *Recent Advances in Electrical and Information Technologies for Sustainable Development*, pp. 173–182, 2019.

[38] I. Ullah and M. Ashraf, "Sliding mode control for performance improvement of shunt active power filter," *SN Applied Sciences*, vol. 1, no. 6, May 2019, doi: 10.1007/s42452-019-0554-9.

[39] D. M. Soomro, S. K. Alswed, M. N. Abdullah, N. H. M. Radzi, and M. H. Baloch, "Optimal design of a single-phase APF based on PQ theory," *International Journal of Power Electronics and Drive Systems (IJPEDS)*, vol. 11, no. 3, p. 1360, Sep. 2020, doi: 10.11591/ijpeds.v11.i3.pp1360-1367.

BIOGRAPHIES OF AUTHORS

Youssef Oubail was born in Agadir, Morocco in 1994. He received engineering degree in industrial engineering in 2017 from the national school of applied sciences, Ibn zohr University, Agadir Morocco. He is currently pursuing PhD degree at in Laboratory of Engineering Sciences and Energy with the national school of applied sciences, Ibn Zohr University, Agadir Morocco. His research interest is artificial intelligence for the integration of renewable energies utilized in microgrids topologies. He can be contacted at email: youssef.oubail@edu.uiz.ac.ma.

Imad Aboudrar was born in Agadir, Morocco in 1993. He is a professor of Electrical Engineering at EST of Dakhla, Ibn Zohr University. He received the M.Sc. degree in electrical engineering in 2016 from the Mohammed V University, Rabat-Morocco, where he obtained his PhD degree at the department of electrical engineering in 2021. His research interests are related to renewables energies, his current activities include the improvement of energy quality of integrated PV/Wind Hybrid Systems utilized in microgrids topologies. He can be contacted at email: aboudrar.imaad@gmail.com.

Mohamed El Hafydy was born in Zagora, Morocco in 1982. He received Master's degree in process and analysis for air quality treatment in from Faculty of Science, Ibn Zohr University, Agadir Morocco. He is currently pursuing PhD degree at in Laboratory of Engineering Sciences and Energy with the National School of Applied Sciences, Ibn Zohr University, Agadir Morocco. His research interest is artificial intelligence for microgrid management. He can be contacted at email: mohamed.elhafydy@edu.uiz.ac.ma.

Elmoutawakil Alaoui My Rachid PhD at the University Ibn Zohr Agadir, Morocco, with a Bachelor in Electronics ENSET, Rabat and Masters in Industrial Engineering at the ENSA Agadir. His doctoral thesis focused on the Defensive Software processors. Permanent member in Engineering Sciences Laboratory and Energy management. Responsible of Industrial Systems Optimization Research Team. Agadir, Morocco. He can be contacted at email: r.alaoui@uiz.ac.ma.

Elmahni Lahoussine PhD in Electrical Engineering and Renewable Energy. Winner of ENSET Rabat in 1993. Member of the Laboratory of Materials and Renewable Energy (RMEL), Professor at the Faculty of Science, Ibn Zohr University, Agadir. His research is focused on Smart Grid, electric vehicles, demand response, energy efficiency, renewable energy integration, energy storage and distributed resources. He can be contacted at email: l.elmahni@uiz.ac.ma.